Journal of Physics: Conference Series

PAPER • OPEN ACCESS

Wind-turbine wakes responding to stably stratified flow over complex terrain

To cite this article: Antonia Englberger and Andreas Dörnbrack 2018 *J. Phys.: Conf. Ser.* **1037** 072014

View the article online for updates and enhancements.

Related content

- Qualitative analysis of wind-turbine wakes over hilly terrain
A Hyvärinen and A Segalini
- Numerical Study of the Impact of Atmospheric Stratification on a Wind-Turbine Performance
A. Chaudhari, O. Agafonova, A. Hellsten et al.
- Stratified flows over a complex relief
N I Makarenko, J L Maltseva and A A Cherevko

IOP ebooks™

Bringing you innovative digital publishing with leading voices to create your essential collection of books in STEM research.

Start exploring the collection - download the first chapter of every title for free.

This content was downloaded from IP address 62.216.202.98 on 20/08/2018 at 06:23

IOP Conf. Series: Journal of Physics: Conf. Series **1037** (2018) 072014 doi:10.1088/1742-6596/1037/7/072014

Wind-turbine wakes responding to stably stratified flow over complex terrain

Antonia Englberger and Andreas Dörnbrack
Institut für Physik der Atmosphäre, DLR Oberpfaffenhofen, Germany
E-mail: antonia.englberger@dlr.de

Abstract. The wake characteristics of a hill-top wind turbine are investigated by means of large-eddy simulations (LESs) of stably stratified atmospheric boundary-layer (ABL) flows. All simulations are conducted with synchronized turbulent inflow data retrieved from an LES of diurnal cycle-driven boundary-layer flow over homogeneous surface. An investigation of different (weak, moderate, strong) stably stratified flow regimes passing over various 3 D hill configurations with heights up to 50 m reveals that the occurrence of flow separation not only depends on hill properties but also on the atmospheric stratification. The hill-top wake characteristics of all flow regimes are compared with wakes resulting from the same flow fields passing through the same wind turbine, however, sited on a homogeneous surface. For the same atmospheric stratification the flow over the hill impacts only the near-wake region. In contrast, the stratification impact on the hill-top wind-turbine wake is much more distinct, especially, in the far wake.

1. Introduction

A detailed understanding of wind-turbine wakes is essential to increase the wind-energy contribution to the world-energy demand in the future. In particular, more precise knowledge about the wake of a wind turbine responding to ABL flow under different thermal stratifications in complex terrain is necessary. This will help to extend the lifetime of a wind turbine and to improve the performance of wind farms.

The individual impacts of complex terrain [1], [2] and of the ABL [3], [4], [5], [6] on wind-turbine wakes have been investigated in several studies within the last years. The deformation of the wind while passing over hilly terrain increases the turbulence and advects it leewards into possible wind-turbine wakes [1], [2]. Considering the ABL, the ambient turbulence impacts the fatigue loading of a wind turbine and controls the entrainment of ambient air into the wake and, therefore, its characteristics. Its intensity is strongly affected by the thermal stratification and the vertical shear of the horizontal wind. Generally, a more rapid wake recovery is observed under convective conditions during the day compared to night-time periods [3], [4], [5], [6]. Transitional periods in the evening and the morning follow the respective flow regime prior to the transition [6].

Both impact factors raise the question, how the wind-turbine wake behaves in the presence of complex terrain under different thermal stratifications. The numerical study presented in this paper focuses on the wind-turbine wake characteristics, influenced by a turbulent flow over a 3 D isolated hill for different stably stratified ABL regimes.

Content from this work may be used under the terms of the Creative Commons Attribution 3.0 licence. Any further distribution of this work must maintain attribution to the author(s) and the title of the work, journal citation and DOI.
Published under licence by IOP Publishing Ltd

2. Framework

2.1. Numerical model setup

The ABL flow over a 3 D hill interacting with a wind turbine is simulated with the multiscale geophysical flow solver EULAG [7]. The model integrates the non-hydrostatic Boussinesq equations of motion and continuity in terrain-following coordinates

$$\frac{d\mathbf{v}}{dt} = -G\boldsymbol{\nabla}\left(\frac{p^{'}}{\rho_0}\right) + \mathbf{g}\frac{\Theta^{'}}{\Theta_0} + \frac{\mathbf{F}}{\rho_0}, \tag{1}$$

$$\frac{d\Theta^{'}}{dt} = -\mathbf{v}\nabla\Theta_e, \tag{2}$$

$$\boldsymbol{\nabla}\cdot(\rho_0\overline{G}\mathbf{v}) = 0, \tag{3}$$

and solves for the Cartesian velocity components $\mathbf{v} = (u, v, w)$ and the potential temperature perturbation $\Theta^{'}$, for a flow with constant density $\rho_0 = 1.1\,\mathrm{kg\ m^{-3}}$ and a constant reference value $\Theta_0 = 300\,\mathrm{K}$ [8]. In the set of equations, d/dt, $\boldsymbol{\nabla}$, and $\boldsymbol{\nabla}\cdot$ represent the total derivative, the gradient, and the divergence, respectively. The factor $p^{'}$ represents the pressure perturbation with respect to the background density, and $\mathbf{g}$ is the vector of acceleration due to gravity. The metric coefficients G and the Jacobian of the transformation $\overline{G}$ [9] represent geometric terms that result from the general coordinate transformation into nonorthogonal terrain-following coordinates [7, 10, 11, 12]. $\mathbf{F}$ is the turbine-induced force in the wind-turbine simulations with an axial F_x and a tangential F_Θ component, respectively. They are parameterized with the blade element momentum method as rotating actuator disc with a nacelle [13]. The simulated wind turbine has a diameter D and a hub height of 100 m. The simulated hill is described by Eq. 4:

$$h(x,y) = \frac{H}{\left(\frac{x}{L}\right)^2 + \left(\frac{y}{L}\right)^2 + 1} \tag{4}$$

For the hill, heights H of 25 m and 50 m and slopes S of 0.25 and 0.50 are investigated. S is defined as H/L, with L corresponding to the length of the symmetric hill between H and $H/2$.

In the simulations conducted in this paper, height dependent ambient states $\psi_e(\mathrm{z}) = (u_e(\mathrm{z}), v_e(\mathrm{z}), w_e(\mathrm{z}), \Theta_e(\mathrm{z}))$ enter Eqs. 1 - 3 in the buoyancy term and as boundary conditions. Further, initial conditions are provided for u, v, w, and the potential temperature perturbation $\Theta^{'}$ in $\psi = (u, v, w, \Theta^{'})$.

2.2. Simulation strategy

All simulations presented in this paper are performed with open streamwise and periodic spanwise boundary conditions and are conducted with synchronized turbulent inflow data of a diurnal cycle-driven boundary-layer flow over homogeneous surface on 512 × 512 × 64 grid points with a resolution of 5 m. This precursor simulation was initialised with a geostrophic wind of 10 m $\mathrm{s^{-1}}$ in streamwise direction and zero for the lateral and vertical wind components and evolved in response to the sensible heat flux provided at the horizontally homogeneous surface over 30 h [6]. Figure 1(a) illustrates the temporal evolution of the streamwise wind component u_e in the course of the day at three heights of 50 m, 100 m, and 150 m, representing bottom tip, hub height, and top tip of a common wind turbine. For three specific times, Figs. 1(b) and (c) show the horizontally averaged height-dependent profiles of $u_e(\mathrm{z})$ and the total turbulent intensity $I(\mathrm{z})$, defined according to Eq. 5

$$I_{i,j,k} = \frac{\sqrt{\frac{1}{3}(\sigma^2_{u_{i,j,k}} + \sigma^2_{v_{i,j,k}} + \sigma^2_{w_{i,j,k}})}}{\overline{u_{i,j,k_h}}}, \tag{5}$$

with $\sigma_{u_{i,j,k}} = \sqrt{\overline{u'^2_{i,j,k}}}$, $\sigma_{v_{i,j,k}} = \sqrt{\overline{v'^2_{i,j,k}}}$, and $\sigma_{w_{i,j,k}} = \sqrt{\overline{w'^2_{i,j,k}}}$, as well as $u'_{i,j,k} = u_{i,j,k} - \overline{u_{i,j,k}}$, $v'_{i,j,k} = v_{i,j,k} - \overline{v_{i,j,k}}$, and $w'_{i,j,k} = w_{i,j,k} - \overline{w_{i,j,k}}$. The indices of the grid points are denoted by i, j, and k in the x, y, and z directions, respectively, and the index k_h corresponds to the hub height.

In this paper, the state of the diurnal cycle situation after 24 h is considered as stable boundary layer (SBL) case, after 29 h as morning boundary layer (MBL) case, and after 18 h as evening boundary layer (EBL) case, following [6].

The initial conditions ψ and the background conditions ψ_e(z) of the LESs performed in the scope of this work, are taken from the corresponding ABL regimes after 18 h, 24 h, and 29 h of the diurnal cycle precursor simulation. Figure 1(d) shows the profiles of ψ_e applied in the wind-turbine simulations of the SBL case. The synchronized coupling between the SBL evolution and the wind-turbine simulations between 24 h and 25 h is realised by providing two-dimensional y-z slices of ψ from the diurnal cycle precursor simulation as upstream values of ψ at the left-most plane of the numerical domain at each time step in the wind-turbine simulations. Figures 1(e) and (f) illustrate them for u and v, taken at the lateral centre of the domain.

With this setup, the wind-turbine wake response to different stably stratified flow of the SBL, the MBL, and the EBL is simulated by three different types of experiments (A, B, and C (Figs. 1(h) - (j))).

Type A Stably stratified flow over a homogeneous surface with a wind turbine as in [6].

Type B Stably stratified flow over a 3 D hill without a wind turbine.

Type C Stably stratified flow over a 3 D hill with a wind turbine on its top.

For simulation types B and C, the sensitivity of the results to varying heights and slopes of the hill (Fig. 1 (g)) is also investigated.

3. Results

In each following simulation, the time period is long enough for the wake to reach an equilibrium state with statistical convergence of the results. All mean values are averaged over the last 50 min of a 60 min simulation. Generally, the numerical simulation results are plotted in dimensionless coordinates as a function of the rotor diameter D.

3.1. Type A

The impact of the SBL on the wind-turbine wake over homogeneous surface is shown in Fig. 1(h) for simulation type A. The wake structure shows a minimum of the velocity magnitude right behind the rotor with a velocity increase in radial and streamwise direction, a pattern resulting from the entrainment of surrounding air with higher velocity values. The non-axisymmetric profile results from the vertical sheared upstream wind profile and the Ekman spiral (Fig. 1(d)). For a more detailed discussion see [6]. The wind-turbine wakes over homogeneous surface corresponding to the MBL and the EBL are comparable to the SBL, with a slightly longer (shorter) wake extension and larger (smaller) velocity deficit values for the MBL (EBL). This is also discussed in more detail in [6].

3.2. Type B

For simulation type B, we refer to nine simulations with varying hill properties (H, S) and ABL (SBL, MBL, EBL) conditions, comparing them to the corresponding simulation over homogeneous terrain. A detailed overview of the type B simulations is given in Table 1.

As first step, we will discuss the characteristics of the velocity profile in relation to the hill position. Following [1], we define a speed up effect as a velocity increase, and a blockage effect

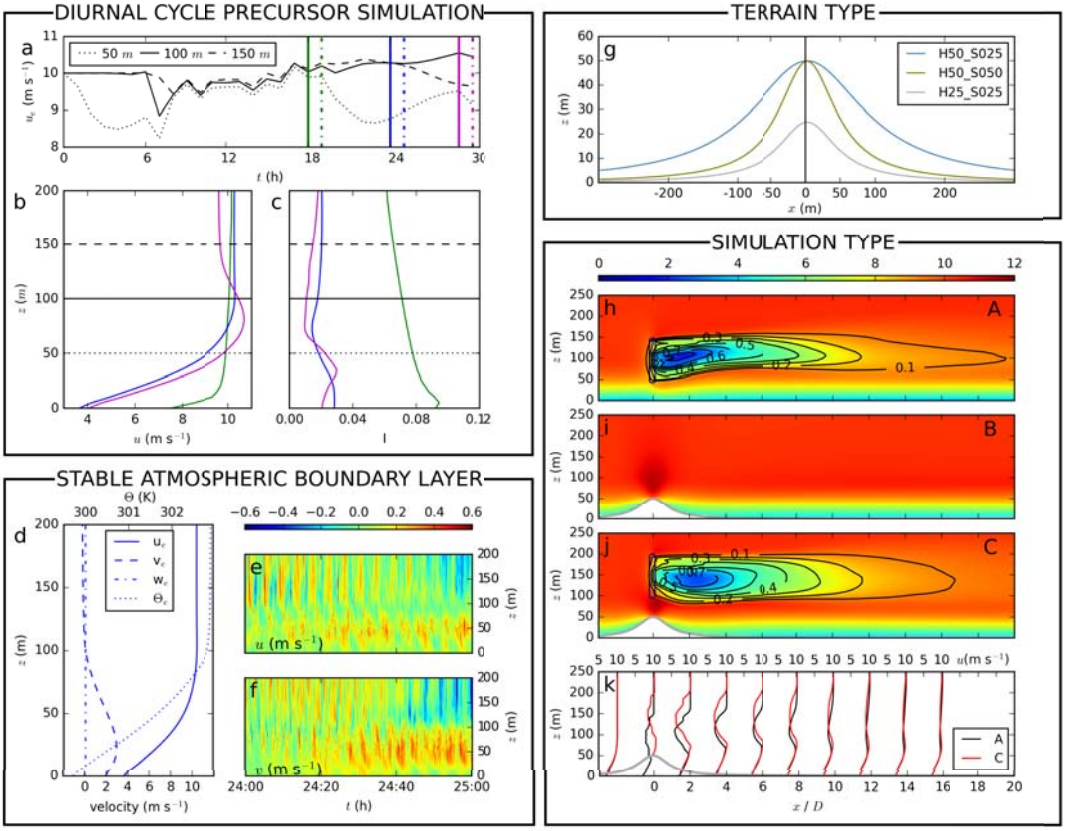

Figure 1. Simulation strategy: Streamwise wind component u_e horizontally averaged at 50 m, 100 m, and 150 m altitude in (a), representing the temporal evolution of the DIURNAL CYCLE PRECURSOR SIMULATION and vertical profiles of u_e in (b) and of the total turbulent intensity I in (c) at specific times of the diurnal cycle. Vertical profiles of u_e, v_e, w_e, and Θ_e after 24 h of the diurnal cycle precursor simulation in (d) and the temporal evolution of the upstream wind profile of u and v in (e) and (f) at the centre of the domain in y-direction, represent the STABLE ATMOSPHERIC BOUNDARY LAYER. The hill heights for three TERRAIN TYPEs at different x- or y-locations from the hill top (symmetric 3 D hill) in (g). Vertical cross sections of $\overline{u_{i,j_0,k}}$ in m s^{-1}, averaged over the last 50 min each, for SIMULATION TYPEs A in (h), B in (i), and C in (j) ($H = 50$ m, $S = 0.25$). The black contours represent the velocity deficit (defined with the temporal average as $(\overline{u_{1,j_0,k}} - \overline{u_{i,j_0,k}})/\overline{u_{1,j_0,k}}$) at the same spanwise location). The contour of the actuator in the cross-sections further represents the transition to a wind-turbine force of zero. Vertical profiles of u ranging from 0 m s^{-1} to 10 m s^{-1} for simulations of type A and type C up- and downstream of the wind turbine from -2 D to 16 D in (k).

and an adverse pressure gradient effect as a velocity decrease at luv and lee, in each case in relation to the reference velocity profile over homogeneous surface.

A comparison of the streamwise velocity between A_SBL and B_SBL_H50_S025 is given in Figs. 1(h) and (i). It results in a distinct speed up of the flow above the hill with a maximum of u related to the top of the hill.

The streamwise velocity profiles of the SBL simulations of type A and B are shown at the lateral centre of the domain and the hill at horizontal distances of -50 m at luv (Fig. 2(a)) and at 50 m at lee (Fig. 2(g)) of the hill and also at hill top (Fig. 2(d)). Here, $ln(z)$ represents the

Table 1. List of performed simulations with varying hill and ABL conditions.

	H / m	L / m	$\overline{u_H}$ / m s^{-1}	N / s^{-1}	F_*	F_H	F_L
B_SBL_H50_S025	50	50	6.4	0.034	~ 0	3.8	3.8
B_SBL_H50_S050	50	100	6.4	0.034	~ 0	3.8	1.9
B_SBL_H25_S025	25	50	4.9	0.032	~ 0	6.1	3.1
B_MBL_H50_S025	50	50	7.0	0.028	~ 0	5.0	5.0
B_MBL_H50_S050	50	100	7.0	0.028	~ 0	5.0	2.5
B_MBL_H25_S025	25	50	5.4	0.023	~ 0	9.4	4.7
B_EBL_H50_S025	50	50	9.3	0.014	0.20	13.3	13.3
B_EBL_H50_S050	50	100	9.3	0.014	0.20	13.3	6.6
B_EBL_H25_S025	25	50	8.9	0.020	0.28	18.6	8.9

height above the ground, following the corresponding terrain shape of Fig. 1(g).

A blockage effect is prevalent at a hill position of -50 m and an adverse pressure gradient effect at 50 m. The accompanied decrease of velocity is most pronounced in the B_SBL_H50_S050 case in the lowest few metres far below the height of a rotor and results from an interaction of the flow with the hill. The much more pronounced velocity decrease in B_SBL_H50_S050 in comparison to B_SBL_H50_S025 results from the higher absolute altitude at luv and lee (Fig. 1(g)), which leads to a higher velocity value, interacting with the near ground region (Fig. 1(b)).

At the top of the hill, the speed up effect is larger if H is larger (B_SBL_H50_S050 and B_SBL_H50_S025 in comparison to B_SBL_H25_S025) with only little dependence on the steepness of the hill (B_SBL_H50_S050 and B_SBL_H50_S025). This speed up effect is accompanied by a decrease of the total turbulent intensity at this position (not shown here).

The investigation of different hill properties provide reliable simulations of the SBL over complex terrain: Similar speed-up, blockage, and adverse pressure gradient effects as simulated here have been investigated in e.g. [1, 14, 15]. Therefore, the effect of thermal stratifications in complex terrain can be investigated as next step. This is necessary, as the stratification effects on the wind-turbine wake are considerably in the type A simulations over homogeneous surface. Further, the type B simulations can be considered as preparatory work to the type C simulations presented in the next section.

For a classification of the kind of flow over different hill configurations and different ABL types, we assume that the wind, which is influenced by different atmospheric conditions occurring throughout the diurnal cycle (SBL, MBL, EBL), approaches a single, isolated, 3 D hill with hill height H and length L, a velocity averaged over H $\overline{u_H}$, and a friction velocity $u_*^2 = \sqrt{(\overline{u'w'_s}^2 + \overline{v'w'_s}^2)}$, with $'$s$'$ denoting surface values. The different thermal stratifications are quantified by the buoyancy frequency N with $N^2 \equiv \frac{g}{\Theta_0}\frac{\partial \Theta}{\partial z}$. With these parameters, we calculate dimensional Froude numbers

$$F_* = \frac{u_*}{NH},$$
$$F_H = \frac{\overline{u_H}}{NH},$$
$$F_L = \frac{\overline{u_H}}{NL},$$

resulting in atmospheric stratifications, which are classified according to Table 2, following [16].

The dimensionless Froude numbers of our nine simulations of type B are listed in Table 1. Following the classification of Table 2, they correspond to a weakly stable stratification for the

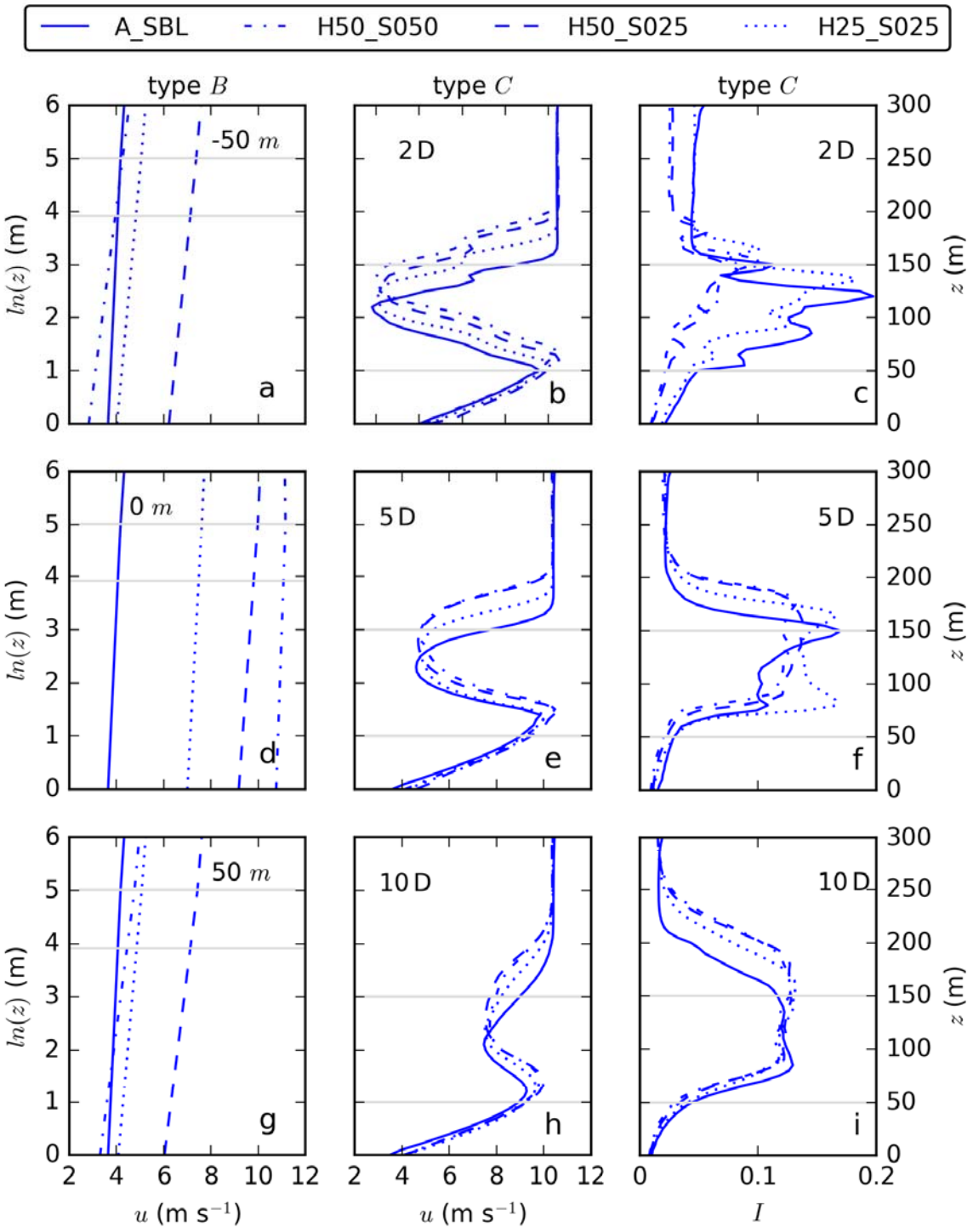

Figure 2. Streamwise velocity profiles of the SBL simulations of type A and B at luv (-50 m) in (a), hill top (0 m) in (d), and lee (50 m) in (g). Further, streamwise velocity (second row) and total turbulent intensity profiles (third row) of type A and C at a downstream distance of 2 D, 5 D, and 10 D in (b), (c), (e), (f), (h), and (i).

Table 2. Classification of dimensionless Froude numbers into different atmospheric stratifications following [16].

	F_*	F_H	F_L
neutral	$>> 1$	$>> 1$	$>> 1$
weakly stable	≤ 1	$>> 1$	$>> 1$
moderately stable	$<< 1$	> 1	≤ 1
strongly stable	$<< 1$	≤ 1	$<< 1$

EBL, the SBL, and the MBL state of the diurnal cycle simulation and for all hill configurations. According to this classification, the impact of the stratification in the type C simulations should be only of minor importance, as all nine simulations of type B can be regarded as weakly stably stratified.

3.3. Type C

For simulation type C, we consider three simulations with varying hill heights and slopes for the SBL regime (C_SBL_H50_S050, C_SBL_H50_S025, C_SBL_H25_S025) and two simulations representing the MBL (C_MBL_H50_S025) and the EBL (C_EBL_H50_S025) for fixed hill geometries of $H = 50$ m and $S = 0.25$.

A comparison of the streamwise velocity is given in Figs. $1(h)$-(j) between A_SBL, B_SBL_H50_S025, and C_SBL_H50_S025. The distinct speed up of the flow above the hill with a maximum of u appearing at the top of the hill is also prevalent in simulation type C. The speed up in type C leads to an acceleration of the flow directly behind the rotor and, therefore, to a velocity deficit maximum located further downstream in comparison to type A. The speed of the far wake (≥ 5 D) recovery is rather comparable up to a velocity deficit of 0.2.

For the flow through the hill-top wind turbine, the actuator disk is faced with an incoming wind profile from another altitude range (100 m to 200 m in type C instead of 50 m to 150 m in type A) with no significant vertical gradient or Ekman spiral. Therefore, the nearly unidirectional flow leads to a more symmetric wake of type C simulations.

Furthermore, the lower edge of the wake bends downward roughly following the terrain as seen more clearly by comparing the shape of the absolute velocity between type A and type C in Fig. $1(k)$. This downward bending of a hill-top wake as response to the stable stratified ABL flow has also been determined in wind-turbine wake measurements [17].

Figures $2(b)$, (e), and (h) represent the vertical profiles of the wake velocity at the lateral centre of the rotor at a downstream distance of 2 D, 5 D, and 10 D. Whereas the height of the velocity minimum depends on the absolute height of the wind turbine, the magnitude of the velocity deficit is comparable for simulations of type A and C. Different hill configurations lead only to minor differences.

The total turbulent intensity I is shown in Fig. 2 for downstream distances of 2 D (Fig. $2(d)$), 5 D (Fig. $2(f)$), and 10 D (Fig. $2(i)$). The values of the vertical profiles through the lateral centre of the rotor at 2 D of type C with $H = 25$ m are much larger than for $H = 50$ m and comparable to the type A values. This effect results from a much less speed up above the hill with $H = 25$ m in comparison to the one with $H = 50$ m. At 5 D, the I-values of C_SBL_H25_S025 are still a little bit larger in comparison to the other type C simulations. This is not longer the case at 10 D. The values are nearly identical for type A and type C simulations. The different vertical region corresponding to the maximum values of I can again be related to the different absolute height of the wind turbine.

An overview of the influence of the hill properties on the wind-turbine wake is shown in Fig. $3(a)$ for the three SBL case simulations. The ratio of the wind speeds of the corresponding

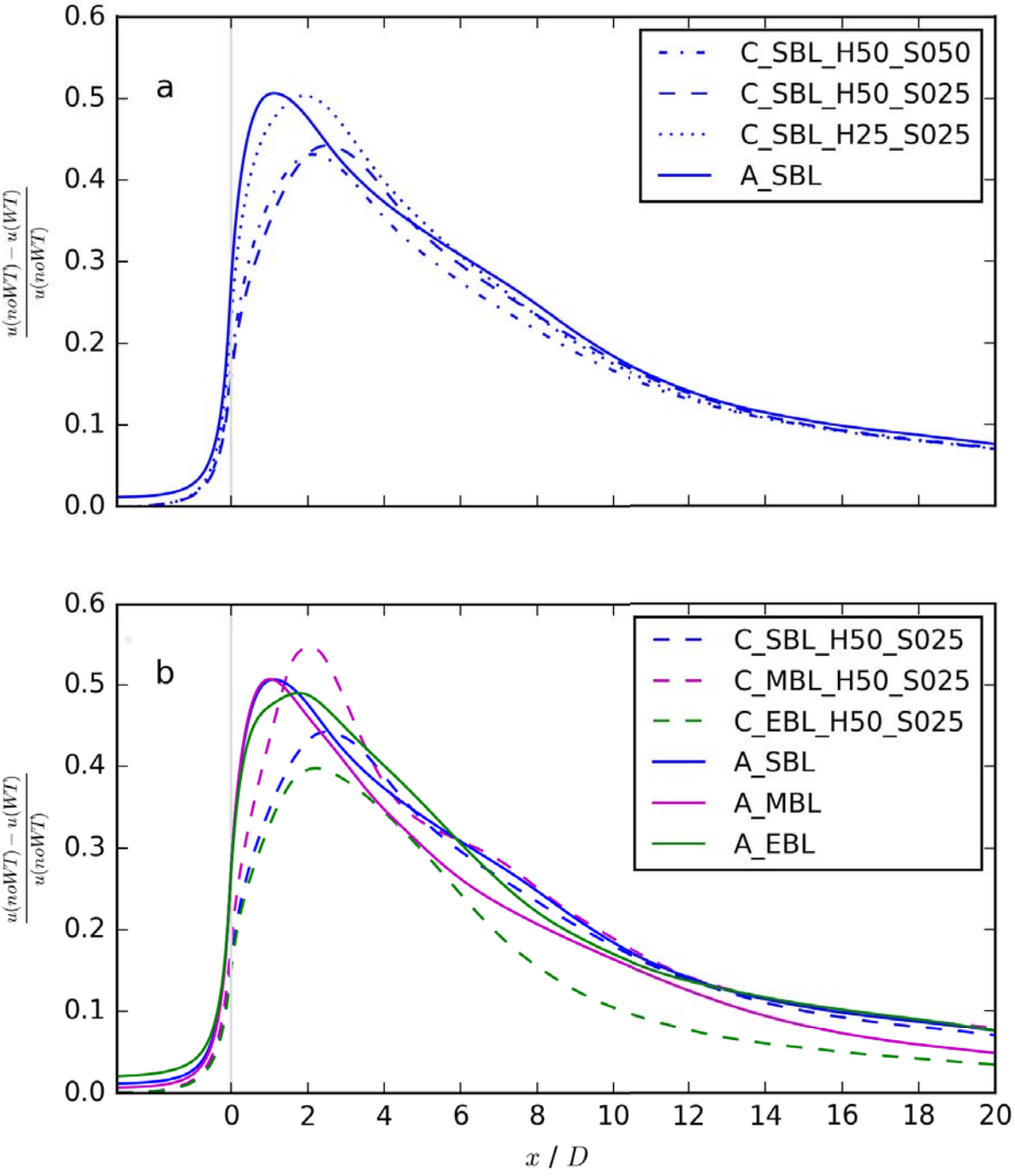

Figure 3. Downstream evolution of the height-averaged ratio of the wind speeds of the corresponding type A, B, and C simulations for different terrain types in (a) and the SBL case, and different stratification types with H = 50 m and S = 0.25 in (b).

type A and type C simulations is calculated at a certain position in the wake as average over the rotor height at the lateral centre of the rotor. For the type A wind-turbine simulation of the SBL, the ratio is calculated between A_SBL and the corresponding diurnal cycle simulation state after 25 h.

A comparison of the ratio between the type A and type C wind-turbine simulations shows a downstream shift of the maximum value for simulations of type C, which increases for increasing H (Fig. 3(a)). Further, the wind speed ratio in the wake is approximately 10% smaller for $H = 50$ m in comparison to $H = 25$ m and to A_SBL. The difference between C_SBL_H25_S025 and A_SBL is only marginal. Likewise, the difference between C_SBL_H50_S050 and C_SBL_H50_S025 is also marginal, with little smaller values for a steeper slope. Consequently, the wake recovers more rapidly for larger H or S-values, induced by the increase of I. This difference in limited to the near-wake region.

In addition to the hill properties, the impact of thermal stratification is investigated in a similar way for $H = 50$ m and $S = 0.25$ (dashed lines in Fig. 3(b)). For all three atmospheric stratifications, the downstream distance at which the maximum of the ratio occurs differs by less than 1 D. Therefore, the location of the streamwise maximum only depends on hill properties. The atmospheric properties, however, modify the absolute values of the ratio. In the SBL case, the magnitude of the ratio and, consequently, the impact of the wind turbine on the atmosphere is smaller in the near wake. In the far wake, however, it is rather comparable up to 20 D. In the MBL case, the impact is larger over the whole wake up to 20 D, whereas in the EBL case it is smaller. This results in a very strong impact of the atmospheric stratification on the wake structure of a hill-top wind turbine up to the far wake.

In summary, the impact of the wind-turbine on the atmospheric velocity and turbulent intensity depends on hill properties and ABL conditions. It intensifies for increasing the height and / or the slope of the hill and also for increasing the atmospheric stability at rotor height. While the terrain impact is limited to the near-wake region, the stratification also influences the far-wake region.

3.4. Discussion

The dimensionless Froude numbers classify the EBL, the SBL, and the MBL regimes of the diurnal cycle simulation as weakly stably stratified atmospheric situations. Therefore, we expected the differences resulting from the stratifications of the EBL, the SBL, and the MBL to be of minor importance for wind-turbine wakes. The differences in the hill-top wind-turbine wakes, however, are significant and seem to depend on the magnitudes of I. In comparison to the SBL, the stratification impact on the wake is smaller (larger) in the EBL (MBL) due to a much larger (smaller) turbulent intensity I over the height of the rotor (Fig. 1(c)). Therefore, a stratification classification in dependence of I results in a weak stably stratified EBL, a moderate stably stratified SBL, and a strong stably stratified MBL. This classification differs from the dimensionless Froude number one, which classifies all three regimes as weakly stably stratified.

4. Conclusion

The flow field over complex terrain and the wake characteristics of a single hill-top wind turbine were studied by means of LESs for different stably stratified flow regimes. The flow fields of an idealised diurnal cycle precursor simulation were used as synchronized atmospheric inflow conditions in complex terrain and hill-top wind-turbine simulations. The turbine-induced forces were parametrized with the blade element momentum method as rotating actuator disc and the hill was realised with terrain following coordinates.

According to this study, a classification only by the buoyancy frequency N or the dimensionless Froude numbers does not seem to be applicable on its own for wind-turbine applications in a height ranging from 50 m to 150 m above the ground. For wind energy purposes, the turbulent intensity of the upstream wind field seem to be much more significant for a stability classification and the resulting stratification effect on the wind-turbine wake. Therefore, the consideration of surface fluxes are not enough to investigate the combined effect

of a hill and a wind-turbine. The advective transport of turbulence seems to be crucial for wind-turbine wake investigations in complex terrain under various atmospheric conditions.

The results of this work highlight the necessity of considering terrain and ABL properties for future wind-turbine wake investigations. To achieve a more detailed understanding of the individual parameters and features, further investigations will be necessary in the future. They will improve rotor configurations and regulation systems, extend the lifetime of a wind turbine, and will further increase the performance of individual wind turbines and wind farms. In the end, it represents an essential next step to increase the wind-energy contribution to the primary energy demand in the future.

Acknowledgments

This work was performed within the project LIPS, funded by the Federal Ministry of Economy and Energy on the basis of a resolution of the German Bundestag under the contract number 0325518. The authors gratefully acknowledge the Gauss Centre for Supercomputing e.V. (www.gauss-centre.eu) for funding this project by providing computing time on the GCS Supercomputer SuperMUC at Leibniz Supercomputing Centre (LRZ, www.lrz.de).

References

[1] Tian W et al 2013 Aerospace Science Meeting (Grapevine: AIAA)
[2] Yang X et al 2015 Phys. of Fluids **27** 025103
[3] Mirocha JD et al 2015 J. of Ren. and Sust. Energy **7** 043143
[4] Abkar M and Porté-Agel F 2014 J. Phys.: Conf. Series **524** p012138
[5] Vollmer L et al 2016 Wind Energy Science **1** 129-141
[6] Englberger A and Dörnbrack A 2017 Bound. Layer Meteorol. https://doi.org/10.1007/s10546-017-0309-3
[7] Prusa JM et al 2008 Comput. Fluids **37** 1193-1207
[8] Smolarkiewicz PK et al 2007 J. Comput. Physics **227** 633-653
[9] Smolarkiewicz PK and Margolin, LG 1998 J. Comput. Physics **140** 459-480
[10] Wedi NP et al 2004 J. Comput. Physics **193** 1-20
[11] Smolarkiewicz PK and Prusa JM 2007 Int. J. Numer. Methods Fluids **47** 789-801
[12] Kühnlein C et al 2012 J. Comput. Physics **7** 2741-2763
[13] Englberger A and Dörnbrack A 2017 Bound. Layer Meteorol. **162** 427-449
[14] Kim HG et al 1997 Wind Eng. Ind. Aerodyn. **66** 17-33
[15] Schulz C et al 2016 J. Phys.: Conf. Series **753** p032016
[16] Carruthers DJ and Hunt JCR 1990 *Atmospheric processes over complex terrain* (Springer) p 83-107
[17] Hansen KS et al 2016 J. Phys.: Conf. Series **753** p032013